Structures 44 (2022) 261–273

Contents lists available at ScienceDirect

Structures

journal homepage: www.elsevier.com/locate/structures

Random forest-based algorithms for accurate evaluation of ultimate bending capacity of steel tubes

Mohamed El Amine Ben Seghier [a], Vagelis Plevris [b,*], German Solorzano [c]

[a] Department of Building and Real Estate, The Hong Kong Polytechnic University, Hung Hom, Hong Kong
[b] Department of Civil and Architectural Engineering, Qatar University, P.O. Box: 2713, Doha, Qatar
[c] Department of Civil Engineering and Energy Technology, OsloMet—Oslo Metropolitan University, Pilestredet 35, 0166 Oslo, Norway

ARTICLE INFO

Keywords:
Ultimate bending capacity
Circular steel tubes
Prediction
Random forest
Whale optimization algorithm
Performance index

ABSTRACT

Despite the existence of methods for estimating the behavior of steel circular tubes subjected to pure bending, analytical models are still restricted due to the problem's complexity and significant nonlinearity. Using the random forest (RF) as the basic model, novel intelligent models are constructed to estimate the ultimate pure bending capacity of circular steel tubes in this study. The RF model's parameters are optimized using three nature inspired optimization algorithms, namely, the particle swarm optimization (PSO), ant colony optimization (ACO) and whale optimization algorithm (WOA). In the experimental part, a database of 104 tests that comprise 49 and 55 pure bending tests conducted on fabricated and cold-formed steel circular tubes, respectively, are evaluated and utilized to investigate the applicability of the hybrid RF-models. A single RF model is also built for comparative reasons in order to estimate the ultimate pending capacity. Various statistical and graphical measures are used to evaluate the performance of the developed models. The results show that the proposed RF-based nature-inspired algorithms can outperform the original RF predictive model. When the hybrid-RF models were assessed, it was discovered that the RF-WOA performed best. In addition, the influence of each parameter on the prediction findings based on the best RF-model is investigated via sensitivity analysis. Taking into account the overall findings, the hybrid RF-models may be used as powerful tools to predict the ultimate bending capacity of circular steel tubes and may be viable to aid technicians in making proper judgments.

1. Introduction

Circular steel tubes have been among the most popular section profiles chosen by structural engineers, due to their advantageous mechanical properties and characteristics such as double symmetry, among others [1,2]. One of these beneficial characteristics is the comparatively high absorption energy capacity under pure bending conditions [3]. As a result, steel circular tubes are particularly well suited for use in large-scale engineering projects of high importance such as offshore and onshore pipelines and platforms; chemical and nuclear powerplants; earthquake and wind resistant structures. However, the deformation mechanism of steel circular tubes subjected to bending is a highly nonlinear phenomenon characterized by ovalization, in which the circular section progressively deforms into an oval shape [4]. This effect is primarily caused by the tensile and compressive stresses generated throughout its cross section, which results in a significant reduction of stiffness, causing the nonlinear behavior and response [5]. Taking into account the locations, loads, and operating circumstances of these constructions, the ovalization produced by the excess bending capacity of steel circular tubes might result in unintended consequences such as failures, causing severe environmental and economic repercussions. In this context, finding a more precise model for estimating the ultimate pure bending capacity of circular steel tubes is critical in order to effectively evaluate and manage the safety of projects that use these structural components.

As conducting experimental tests is costly, time-consuming, and necessitates the use of specific designed test rigs, utilizing design codes and standards to estimate the bending moment capacity is a typical practice. As a result, various closed-form solutions to consider the ovalization mechanism in circular steel tubes have been presented in the literature during the previous few decades. Among the most well-known codes and standards for predicting the ultimate bending capacity of circular hollow steel tubes are Eurocode 3 [6], AS/NZS 4600 [7], AS 4100 [8], and AISC [9]. Most of these approaches are only effective for

* Corresponding author.
E-mail addresses: mohamed.benseghier@polyu.edu.hk (M.E.A. Ben Seghier), vplevris@qu.edu.qa (V. Plevris), germanso@oslomet.no (G. Solorzano).

https://doi.org/10.1016/j.istruc.2022.08.007
Received 24 April 2022; Received in revised form 9 July 2022; Accepted 1 August 2022
Available online 9 August 2022

cases with a small degree of ovalization based on the assumption that the ovalized form is a perfect ellipse [10–12]. Other approaches have been also developed and proposed for higher degrees of ovalization, by adding additional assumptions, such as considering plastic hinges at certain positions along the tube length [13] or a linear distribution of the plasticity over the whole element [2]. Highly detailed finite element models, on the other hand, may be more trustworthy and attain better accuracy for both small and large degrees of deformation, as shown in [14–16]. Nonetheless, the simulation becomes challenging and computationally costly because of the needed detail and the consequent high complexity of the model [17]. Although all the aforementioned methodologies are capable of capturing the response of steel tubes to some extent, their applicability is restricted due to the various assumptions and simplifications utilized in their mathematical formulations. Soft computing techniques, on the other hand, offer greater flexibility because they do not need a rigid mathematical representation, and hence no assumptions or simplifications on the underlying phenomena are required.

Artificial intelligence (AI) methodologies are becoming a popular trend for solving engineering challenges by building more generic models that do not require any explicit physics or assumptions about the databases they rely on [18–21]. While hard-computing models use experimental data to calibrate a mathematical formulation given some specific assumptions, AI models, widely known as soft-computing models directly use the given data to find proper patterns and create a predictive data-driven model to find approximate solutions, requiring only a few user-defined parameters (also known as hyperparameters) to control the algorithm's performance. Various types of AI approaches have been well established as strong and reliable alternatives to predicting the complex behavior between input parameters and expected outputs, including the use of machine learning (ML) techniques, such as artificial neural network and support vector regression; ensemble learning (EL) techniques such as random forest, adaptive boosting and extreme gradient boosting; and deep learning (DL) techniques such as deep neural network. These and other relevant AI approaches have been recently widely used to solve a variety of complex engineering problems, such as predicting the shear strength of steel fiber unconfined concrete [22], predicting the masonry failure under biaxial stress [23,24], modeling degradation in steel structures [25–27], estimating the axial capacity of square concrete-filled steel tubular columns [28], analyzing the axial compression capacity of circular concrete-filled steel tube columns [29], modeling the maximum ultimate bond strength between the corroded steel reinforcement and surrounding concrete [30], and many other applications in structural engineering [31]. Yet only few research works have been undertaken utilizing soft-computing methodologies to handle the engineering challenges discussed in the present work. Shahin and Elchalakani [32] are regarded as one of the first to have used an artificial neural network to estimate the ultimate bending capacity, with findings indicating that the suggested AI-based model outperformed the existed codes and standards. Basarir et al. [33] estimated the ultimate pure bending of concrete filled tubes and regular steel tubes using neuro-fuzzy inference algorithms and neural networks, respectively. The study demonstrates the significance and promising outcomes produced by utilizing AI-models in comparison to analytical models. Among the soft-computing models, it was discovered that EL models outperform single ML-models, as the previous uses a single ML-model as the weak learner to estimate the overall EL-model performance (strong learner) [34]. Xu et al. [35] investigated seven soft computing algorithms for predicting the capacity of steel tubular columns and discovered that random forest produces the best results. RF is a simple, yet powerful model that can handle complex databases and is considered computationally lighter than other EL-models (e.g. Adaboost and XGBoost) [36,37].

All the aforementioned AI-models are used as independent models, with their hyper-parameters chosen manually. To improve AI model performance and overcome this limitation, *meta*-heuristic optimization methods can be used as hybrid AI-models for the automatic selection of the controlling parameters. In this study, we propose, test, and compare three different variants of a novel soft computing-based methodologies for modeling the complex behavior of the ultimate pure bending capacity of circular steel tubes. This will enable the development of an accurate solution in comparison to the existing codes and correlations. Each of the proposed variants is based on the random forest (RF) approach due to its advantages, which is paired together with a secondary nature-inspired optimization algorithm to automatically determine its control parameters in an optimal way. The selected nature-inspired optimization algorithms include the particle swarm optimization (PSO), ant colony optimization (ACO), and whale optimization algorithm (WOA). These metaheuristics have been used in a variety of problems in structural engineering with very impressive results [38–41]. As a result, three novel hybrid strategies emerge, namely (i) RF-PSO, (ii) RF-ACO and (ii) RF-WOA. The models are constructed based on experimental results from cold-form and fabricated circular steel tubes subjected to pure bending conditions, with a total of 104 tested elements comprising the database used for training and testing processes. The developed hybrid RF-models' accuracy and agreement predictions are compared to the ones obtained from regular RF-models, and the highest performing model is compared to pre-existing standards utilized for predicting the ultimate bending capacity. The remainder of the manuscript is structured as follows: Section 2 describes the technique for conducting the experimental tests, as well as the database description and the used statistical metrics. Section 3 discusses the suggested hybrid RF-models, whereas Section 4 discusses the implementation stages. Section 5 reports and discusses in depth the results of the implemented hybrid framework. Section 5 concludes with the primary findings and recommendations.

2. Experimental set up and database description

2.1. Experimental test description

The database used in this study to train the corresponding models is obtained from a variety of sources in the literature, and it comprises the results of 104 experimental tests of circular steel tubes subjected to pure bending. From the complete list, 49 of the specimens are fabricated (also known as structural steel tubes), while the remaining 55 are cold-formed tubes. From the 49 tests carried on fabricated steel tubes, 27 are taken from the work by Sherman [42,43], 10 from experiments conducted by Schilling [44], 4 from the work of Jirsa et al. [45], and 8 from Korol and Huboda [46]. The remaining 55 experiments, regarding the cold-formed tubes, are taken from the studies conducted by Elchalakani et al. [47,48].

The standard testing setup comprises of a customized rig intended to deliver pure bending conditions over the test specimen's central span without causing considerable axial or shear forces. This is accomplished by applying the loading with the help of two revolving wheels and two fixed support points. Fig. 1 depicts a schematic diagram of the experimental test setup. Using different sensors and measurement equipment, the moment–curvature (M–κ) is calculated by detecting the angular rotation κ and estimating the related bending moment. Elchalakani provides a detailed explanation of the testing procedure in [47].

2.2. Data sets description

The data from the 104 experimental tests are processed to generate a valid dataset with specified inputs and outputs that can be used in the numerical investigations. Each experimental test represents a data point with four input parameters and a single output parameter. The four input variables characterize the physical attributes of the tested specimen, and are namely the following: (1) the thickness t of the section, (2) its diameter d, (3) the yielding stress of the fabrication steel f_y, and (4) its elastic modulus E. The output parameter value (result) is equal to the

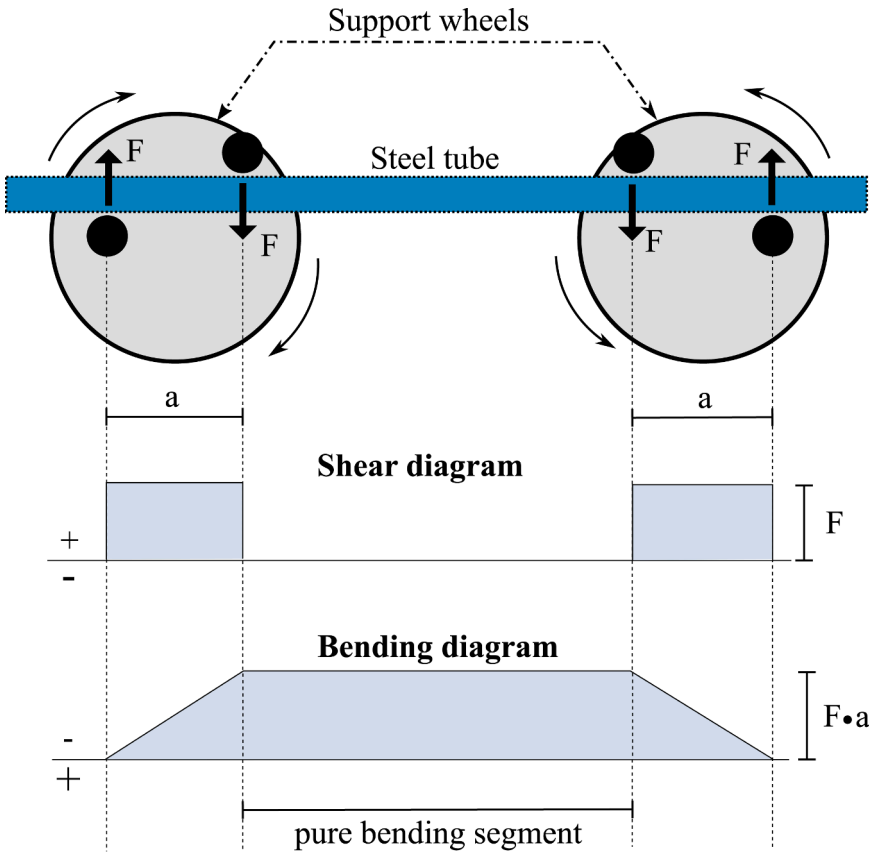

Fig. 1. Schematic of the experimental test set up.

measured ultimate bending moment M_u. The complete database is displayed in two separate tables. Table 1 relates to the 49 fabricated steel tubes, whereas Table 2 corresponds to the 55 cold-formed steel tubes.

2.3. Data sets analysis

A statistical analysis is performed on the database, and the following statistical quantities are extracted for each variable: the minimum value (MIN), the maximum value (MAX), the range (RNG), the mean value (MEAN), and the standard deviation (SD). Tables 3 summarizes the statistical analysis findings for the fabricated and cold-formed and overall tubes, respectively. It can be noted that the fabricated-type steel tubes constitute the larger specimens, with a mean diameter and thickness of 344 mm and 7.87 mm, respectively, whereas the cold-formed-type tubes represent smaller ones, with a mean diameter and thickness of 80.99 mm and 2.43 mm, respectively. Furthermore, the table findings show that the output variable, M_u, ranges between 0.8 and 480.63 kN•m. Fig. 2 also depicts the correlation matrix of the whole database that was used. The plots of this figure comprise histograms of the input and output variables, as well as the coefficients of correlation between them. The histograms in Fig. 2 indicate the data's random distribution based on pre-defined intervals, whereas the crossplots show the agreement between the variables. M_u clearly correlates with the wall thickness and diameter, with correlation values equal to 0.91 and 0.86, respectively. M_u, on the other hand, has a negative correlation (−0.16) with the yielding stress of the manufacturing steel and similarly a negative correlation (−0.11) with the elastic modulus, showing an inverse weak correlation. According to the statistical indicators, both the input and output variables have distinct ranges and scales, as well as a varied degree of correlation, indicating the difficulty and the challenges imposed in modeling the ultimate capacity of pure bending for circular steel tubes.

3. Proposed modeling framework

3.1. Random forest

The Random Forest (RF) is a strong Ensemble Learning (EL) methodology established by Breiman [49] that is based on combining the bagging ensemble learning theory [50] with Ho's random subspace method [51]. The decision tree (DT) has a basic structure as the RF's fundamental for prediction problems, however, DT suffers from overfitting when the input variables are rather complicated. As a result, DT will be unable to adequately deal with categorization issues. Thus, RF offers a higher generalization capacity and a better prediction result than the classic DT model [34]. The RF model randomness is mostly evident in the two elements listed below. To begin, the bootstrap approach is used to randomly choose K new sample sets using the training set based on the model inputs, whereas each new sample set is utilized to train a DT. As a result, the RF model has K DTs as the basis estimator. The out-of-bag (OOB) datasets are made up of the unselected samples. Second, during DT building, a specified number of features (N) of the input variables have to be randomly extracted. Each DT will produce an estimated result for prediction problems, while all prediction results of the K DTs will be voted on to decide the final prediction RF outcomes. The RF model's final decision outcome is provided below [52]:

$$H(\boldsymbol{X}) = \arg max \sum_{i=1}^{K} I(h_i(\boldsymbol{X}) = \boldsymbol{Y}) \quad (1)$$

where H(X) denotes an RF model with various DTs; h_i is the *i-th* individual DT; K is the total DTs number; and **X** and **Y** represent the vectors

Table 1
Experimental tests results for the 49 fabricated circular tubes.

Fabricated tubes	Inputs				Output
Reference	t (mm)	d (mm)	f_y (MPa)	E (MPa)	M_u (kN·m)
[42]	26.6	457	279	199,630	1442.1
[42]	18.7	457	299	199,899	1237
[42]	16.5	458	338	200,359	1198.1
[42]	13.1	458	299	200,353	830.9
[42]	9.9	458	294	200,590	562.9
[42]	6.9	458	325	199,433	381.5
[42]	6.1	456	314	200,909	346.6
[42]	6.3	456	309	201,066	358.6
[42]	12.9	610	314	200,080	1490.1
[42]	6.8	610	373	201,196	810.4
[42]	25.4	457	374	199,940	1892.7
[42]	19.6	458	390	199,859	1408.6
[42]	18.8	455	367	198,943	1391.7
[42]	16.4	458	424	199,920	1302.9
[42]	13.3	458	411	199,931	1111.5
[42]	10	458	410	200,485	783.4
[42]	6.8	458	434	199,501	538.8
[42]	13.6	610	405	199,138	1729.7
[42]	13.7	608	378	199,720	1828.2
[42]	7	609	429	200,617	918.3
[42]	9.9	608	401	200,251	1317.2
[43]	14.9	273	290	210,000	306.1
[43]	7.8	273	304	210,000	160
[43]	5.6	273	405	210,000	150.9
[43]	4.9	273	419	210,000	139.7
[43]	3.5	273	287	210,000	64.7
[43]	2.5	273	311	210,000	48.8
[44]	1.9	109	269	210,000	7.1
[44]	1.4	103	270	210,000	4.3
[44]	1.1	105	270	210,000	3.2
[44]	0.94	103	245	210,000	2.3
[44]	0.76	104	267	210,000	1.6
[44]	2.9	100	358	210,000	10.3
[44]	2.3	125	359	210,000	12.2
[44]	1.6	112	357	210,000	7.4
[44]	0.99	89	370	210,000	2.7
[44]	1.3	117	394	210,000	6.2
[45]	5.9	273	380	210,000	167.2
[45]	8.9	273	334	210,000	232.1
[45]	6.6	406	342	210,000	385.7
[45]	6.5	508	375	210,000	593.1
[46]	3.9	114	308	210,000	15.4
[46]	3.9	168	305	210,000	33.2
[46]	4.8	168	368	210,000	48.3
[46]	5.6	273	306	210,000	126.7
[46]	6.4	324	377	210,000	248.9
[46]	6.4	356	297	210,000	231.3
[46]	6.3	406	309	210,000	297
[46]	6.4	508	362	210,000	509.5

Table 2
Experimental tests results for the 55 cold-formed circular tubes.

CF tubes	Inputs				Output
Reference	t (mm)	d (mm)	f_y (MPa)	E (MPa)	M_u (kN·m)
[47]	2.53	101.8	365	199,800	8.8
[47]	2.6	88.6	432	209,500	8
[47]	2.45	76.3	415	217,100	5.1
[47]	3.35	89.3	412	217,900	9.9
[47]	2.44	60.6	433	211,100	3.1
[47]	3.24	76.2	456	211,100	7.6
[47]	3.01	60.6	408	204,700	4.2
[47]	1.98	33.6	442	204,200	0.8
[47]	2.63	33.8	460	207,100	1.1
[48]	1.1	110.1	408	190,900	3.9
[48]	1	109.9	408	190,900	3.7
[48]	0.9	109.7	408	190,900	3.4
[48]	1.25	110.4	408	190,900	4.5
[48]	1.7	98.6	410	212,300	5.8
[48]	1.2	98.8	404	191,200	4.3
[48]	1.4	99.2	404	191,200	4.9
[48]	1.6	99.6	365	199,800	5.4
[48]	1.8	100	365	199,800	5.3
[48]	2.3	99.8	410	212,300	8.9
[48]	2.4	87.3	412	217,900	5.7
[48]	2.1	100.6	404	191,200	7.5
[48]	2.44	101.8	365	200,000	8.7
[48]	2.52	89.3	378	182,000	6.4
[48]	2.17	76.3	415	217,000	4.7
[48]	3.1	89.3	412	218,000	9.4
[48]	2.23	60.7	433	211,000	3
[48]	3.07	76.2	456	211,000	7.7
[48]	2.9	60.7	408	205,000	3.7
[48]	2.4	33.8	460	207,000	1.1
[48]	2.44	101.8	365	200,000	8.4
[48]	2.44	101.8	365	200,000	8.7
[48]	2.52	89.3	378	182,000	6.7
[48]	3.08	89.1	473	201,000	10
[48]	2.29	60.2	407	211,000	3.3
[48]	3.07	76.2	456	211,000	7.4
[48]	2.95	60.37	413	196,000	4
[48]	2.54	101.1	400	190,000	10.5
[48]	2.52	89.3	378	182,000	7.2
[48]	2.35	76.1	370	202,000	4.6
[48]	3.08	89.1	473	201,000	10.6
[48]	2.29	60.2	407	211,000	3.3
[48]	3.13	75.9	402	198,000	6.7
[48]	2.95	60.4	413	196,000	4.3
[48]	2.52	89.3	378	182,000	7.3
[48]	2.29	60.23	407	211,000	3.8
[48]	2.95	60.4	413	196,000	4.6
[48]	2.54	101.1	400	190,000	8.7
[48]	2.52	89.3	378	182,000	6.4
[48]	2.35	76.1	370	202,000	4.3
[48]	3.08	89.1	473	201,000	9.8
[48]	2.29	60.2	407	211,000	3.3
[48]	3.13	75.9	402	198,000	5.9
[48]	2.95	60.4	413	196,000	4.1
[48]	2.52	89.3	378	182,000	6.2
[48]	2.95	60.4	413	196,000	4

of the input variables and correct prediction, respectively.

3.2. Optimized random forest using meta-heuristics

The RF features several built-in parameters, including the DTs number in the RF model (n estimators), the minimum number of samples necessary for a node in the tree to split (min samples split), and the maximum depth of the output tree (max depth). These three factors are critical for balancing prediction performance and modeling computational speed. Typically, the trial-and-error approach is used to manually pick these settings. However, in this study-three nature inspired optimization algorithms are utilized in order to auto-select these parameters, namely Particle Swarm Optimization (PSO), Ant Colony Optimization (ACO) and Whale Optimization Algorithm (WOA). The following sections cover the specifics of the suggested hybrid models.

3.2.1. Particle swarm optimization (PSO)

PSO is a well-known population-based algorithm developed by Kennedy and Eberhart [53] in response to the dynamic movements and associated communications of animals such as flocks of birds or schools of fish. PSO's searching mechanism iteratively updates a population (swarm) of probable solutions known as particles. The particles with their respective coordinates in the multidimensional search space represent possible solutions to the optimization problem, where each particle is labelled with its position and velocity. The appropriate position and velocity in the D-dimensional space for a particle i at iteration k are stated as follows:

$$\boldsymbol{X}_{i,k} = \{\boldsymbol{X}_{i1}, \boldsymbol{X}_{i2}, \cdots, \boldsymbol{X}_{iD}\} \tag{2}$$

$$\boldsymbol{v}_{i,k} = \{\boldsymbol{v}_{i1}, \boldsymbol{v}_{i2}, \cdots, \boldsymbol{v}_{iD}\} \tag{3}$$

where $\boldsymbol{v}_{i,k}$ and $\boldsymbol{x}_{i,k}$ denote the velocity and position of the i-th particle at iteration k, respectively. The velocity of each particle varies in each

Table 3
Statistical quantities of the fabricated circular tubes test results.

Data sets	Statistics	Inputs				Output
		t (mm)	d (mm)	f_y (MPa)	E (MPa)	M_u (kN·m)
Fabricated tubes	MIN	0.76	89	245	198,943	1.6
	MAX	26.6	610	434	210,000	1892.7
	RNG	25.84	521	189	11,057	1891.1
	MEAN	7.87	344.58	344.29	205878.96	526.15
	SD	5.64	171.05	49.95	4863.52	563.56
Cold-form tubes	MIN	0.9	33.6	365	182,000	0.8
	MAX	3.35	110.4	473	218,000	10.6
	RNG	2.45	76.8	108	36,000	9.8
	MEAN	2.43	80.99	409.69	200759.26	5.78
	SD	0.61	20.14	29.54	10646.68	2.48
Overall data sets	MIN	0.76	33.6	245	182,000	0.8
	MAX	26.6	610	473	218,000	1892.7
	RNG	25.84	576.4	228	36,000	1891.9
	MEAN	5.17	206.47	377.82	203102.12	259.79
	SD	5.24	177.60	52.51	8707.69	480.63

iteration according to the equation below:

$$\boldsymbol{v}_{i,k+1} = \chi^{*}\left(\left(\boldsymbol{v}_{i,k} + c_1 r_1\left(\boldsymbol{pbest}_{i,k} - \boldsymbol{x}_{i,k}\right) + c_2 r_2\left(\boldsymbol{gbest}_{k} - \boldsymbol{x}_{i,k}\right)\right)\right) \tag{4}$$

where $\boldsymbol{pbest}_{D,k}$ signifies the *i-th* particle's best position at the *k-th* iteration;$\boldsymbol{gbest}_{k}$ denotes the best position in the entire swarm, while c_1 and c_2 represent positive acceleration constants and r_1, r_2 uniformly distributed random numbers in the range [0, 1]. χ is known as the convergence factor, which is computed as follows:

$$\chi = \frac{2}{\left|2 - \theta - \sqrt{\theta^2 - 4\theta}\right|} \tag{5}$$

with $\theta = c_1 + c_2 > 4$. Commonly, θ is equal to 4.1, and as a result $\chi = 0.729$. Then, each particle changes its position according to the following equation:

$$\boldsymbol{X}_{i,k+1} = \boldsymbol{X}_{i,k} + \boldsymbol{v}_{i,k+1} \tag{6}$$

The optimal best position for the *i-th* particle and the best swarm individual are changed at $(k+1)$-*th* iteration based on the minimization of the objective function f, throughout the PSO search process, as follows:

$$\boldsymbol{pbest}_{i,k+1} = \begin{cases} \boldsymbol{pbest}_{i,k}, & if \;\; f\left(\boldsymbol{pbest}_{i,k}\right) \leqslant f\left(\boldsymbol{X}_{i,k+1}\right) \\ \boldsymbol{X}_{i,k+1}, & otherwise \end{cases} \tag{7}$$

$$\boldsymbol{gbest}_{k+1} = \min\left\{f\left(\boldsymbol{pbest}_{i,k+1}\right)\right\} \tag{8}$$

In this paper, PSO is used to determine the optimal combination RF parameters (i.e. n estimators, min samples split, and max depth). Fig. 3 depicts the framework of the proposed RF-PSO model.

3.2.2. Ant colony optimization (ACO)

ACO is a nature inspired algorithm proposed by Dorigo and Gambardella [54,55] to solve discrete optimization problems. The algorithm was inspired by the behavior of ants while searching for food. Ants deposit pheromone in varying amounts depending on the quality of food and the path used to get it. ACO has been expanded to continuous domains with a new version using an improved pheromone concept [56]. The first phase in ACO is to generate m ants that represent potential solutions and assess the created ants using the fitness function. Thereafter, the ants are sorted from best to worst in terms of fitness function performance under what is called, solution archive, where the archive solutions are assigned weight values (w_i, where i denotes the i-th ant) [57]. As a result, the following Gaussian function is used:

$$w_i \propto \frac{1}{\sqrt{2\pi}\alpha m} exp\left[-\frac{1}{2}\left(\frac{i-1}{\alpha m}\right)^2\right] \tag{8}$$

where $\sum_{i=1}^{m} w_i = 1$, which denotes the mean, where α is ACO parameter and m is the ants number. Thus, the Gaussian mixture is utilized that is defined as follows [58]:

$$G^{l}(\boldsymbol{X}[l]) = \sum_{i=1}^{m} w_i N(\boldsymbol{X}[l]; \mu_i[l], \sigma_i[l]) \tag{9}$$

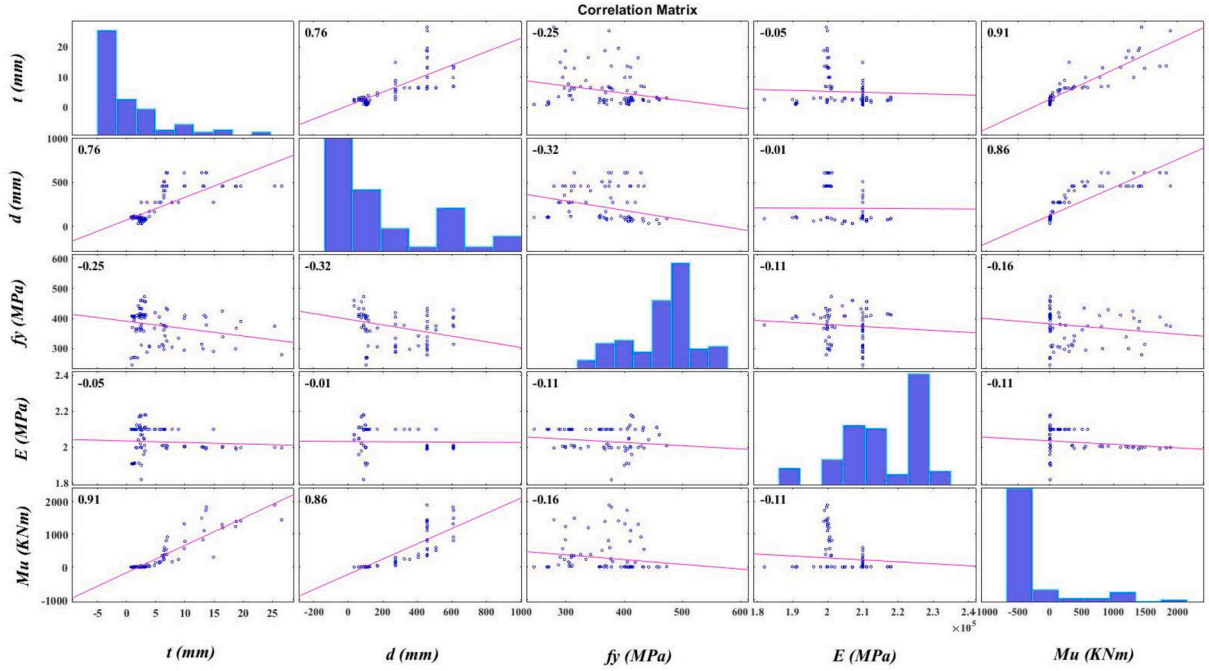

Fig. 2. Correlation matrix of the input and output parameters of the data sets.

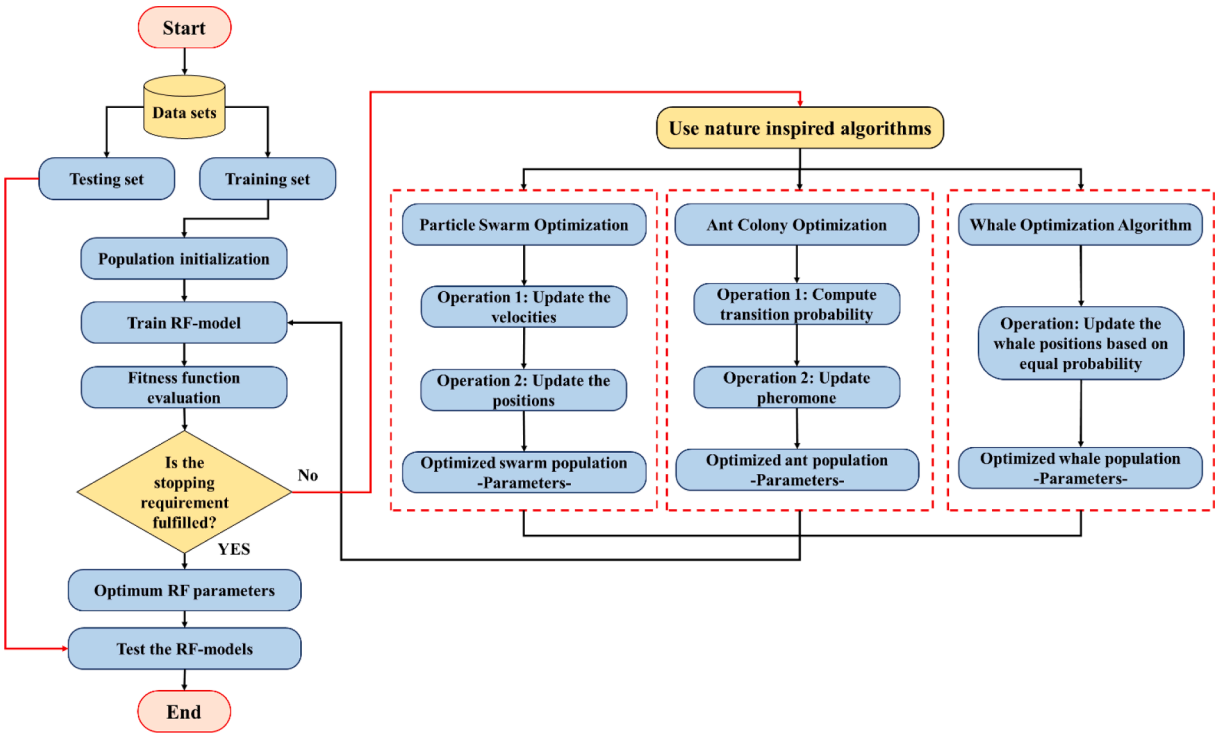

Fig. 3. Framework of the proposed optimized random forest using nature inspired algorithms.

$$N(\boldsymbol{X};\mu,\sigma)=\frac{1}{\sqrt{2\pi}\sigma}exp\left[-\frac{1}{2}\left(\frac{\boldsymbol{X}-1}{\sigma}\right)^2\right] \tag{10}$$

where l denotes the decision variable, while $\boldsymbol{X}[l]$ denotes the l-th element of $\boldsymbol{X}$. Thereafter the mean and standard deviation the Gaussian mixture are calculated as follows:

$$\boldsymbol{\mu}_i[l]=\boldsymbol{X}_i[l] \tag{11}$$

$$\boldsymbol{\sigma}_i[l]=\frac{\delta}{m-1}\sum_{i'=1}^{m}[\boldsymbol{X}_i[l]-\boldsymbol{X}_{i'}[l]\,] \tag{12}$$

Note that δ is a positive parameter to balance the exploitation and exploration phases. A specific number (n) of offspring are acquired by sampling according to the earlier archive. Using these offspring and the predetermined number of fittest solutions, a new archive is created. The problem's best solution is indicated using the best archive element. These phases of searching are iterated until a predetermined termination criterion is met. ACO is coupled with RF model in order to compute its performance parameters. Fig. 3 displays the suggested RF-ACO model's framework.

3.2.3. Whale optimization algorithm (WOA)

WOA is a newly developed global optimization algorithm by Mirjalili and Lewis [59] that was inspired by the hunting behavior of humpback whales which surround their prey with a spiral bubble-net feeding maneuver. The first stage in WOA is to generate a random set of solutions and evaluate the fitness function. The positions of the agents are then repeatedly updated based on the best agent, given some specified requirements. The following equation governs the position update process [60]:

$$\overrightarrow{\boldsymbol{X}}(k+1)=\begin{cases}\overrightarrow{\boldsymbol{X}}^{*}(k)-\overrightarrow{\boldsymbol{A}}.\overrightarrow{\boldsymbol{D}} & if\ p<0.5\\ \overrightarrow{\boldsymbol{D}'}e^{bl}cos(2\pi k)+\overrightarrow{\boldsymbol{X}}^{*}(k) & if p\geq 0.5\end{cases} \tag{13}$$

where k denotes the current iteration and p is a random number in the range [0,1] indicating the chance of shape's position updating (i.e. 50 % circular and 50 % spiral). $\overrightarrow{\boldsymbol{D}'}$ represents the distance vector between the i-th whale (i.e. agent) and the prey $\overrightarrow{\boldsymbol{X}^{*}}$ (i.e. best solutions vector), i.e. $\overrightarrow{\boldsymbol{D}'}=\left|\overrightarrow{\boldsymbol{X}^{*}}(k)-\overrightarrow{\boldsymbol{X}}(k)\right|$. b is a constant used to define the spiral shape, while l is a random number in the range $[-1, 1]$. The vectors $\overrightarrow{\boldsymbol{D}}$ and $\overrightarrow{\boldsymbol{A}}$ are computed as follows:

$$\overrightarrow{\boldsymbol{D}}=\left|\overrightarrow{\boldsymbol{C}}.\overrightarrow{\boldsymbol{X}^{*}}(k)-\overrightarrow{\boldsymbol{X}}(k)\right| \tag{14}$$

$$\overrightarrow{\boldsymbol{A}}=2\overrightarrow{\boldsymbol{a}}.\boldsymbol{r}-\overrightarrow{\boldsymbol{a}} \tag{15}$$

where $\overrightarrow{\boldsymbol{C}}=2\overrightarrow{\boldsymbol{r}}$, where $\overrightarrow{\boldsymbol{a}}$ is a vector that drops linearly from 2 to 0 during the distance course, $\overrightarrow{\boldsymbol{r}}$ represents a random vector in the range [0, 1]. In the above formulas, the · symbol means an element-by-element multiplication of the vectors. Meanwhile, $\overrightarrow{\boldsymbol{A}}$ must be in the interval $[-1,1]$, otherwise, if $\overrightarrow{\boldsymbol{A}}$ is outside of this interval, the position is updated in a circular-based shape on a randomly selected individual $\overrightarrow{\boldsymbol{X}_{rand}}(k)$ as indicated in the following expression:

$$\overrightarrow{\boldsymbol{X}}(k+1)=\overrightarrow{\boldsymbol{X}_{rand}}(k)-\overrightarrow{\boldsymbol{A}}.\overrightarrow{\boldsymbol{D}} \tag{16}$$

The first component of Eq. (13) depicts the adaptation of the encircling process in WOA, whereas the second component of Eq. (13) mimics the bubble-net approach. Because the exploration and exploitation phases are the two fundamental processes of any population-based algorithm, an equal probability p is assumed for both phases and guaranteed by fine-tuning the parameters a and c.

After the coordinates updating, the fitness function is evaluated again, and $\boldsymbol{X}^{*}(k+1)$ is updated if the optimal solution surpasses the previous one $\boldsymbol{X}^{*}(k)$. Finally, this procedure is iterated until a predetermined termination criterion is met. Similar to the previous nature inspired algorithms, WOA is used to automatically select the optimal RF parameters, whereas the suggested RF-WOA framework is depicted in Fig. 3.

3.3. Implementation methodology

3.3.1. Modeling process

Fig. 4 depicts the implementation methodology of the modeling process used in the study, where three major stages are taken to produce the primary conclusions based on the constructed RF-based models. These stages are outlined below:

3.3.1.1. Data preparation and analysis. This phase comprises the data collection and the pre-analysis performed in Section 2. It is critical to compile a solid database with no missing data. Furthermore, the database should be separated into two parts: the training set for developing the hybrid RF-models and the testing set for the validation of the results. Due to the lack of a precise definition for the splitting percentage between the training and testing sets, a trial-and-error technique is used. This approach entails experimenting with several splitting schemes and then analyzing the performance of the models based on the results, to choose the optimal splitting based on the statistical criteria mentioned in Section 3.3.2. Three distinct random splitting techniques are suggested as 90–10 %, 80–20 % and 70–30 % for the training and testing sets, respectively.

3.3.1.2. Development of RF-models. After constructing the training and testing data sets based on the previous random splits, the modeling procedure begins as described in Section 3.2. Noting that the trial-and-error method is also employed for the standalone RF model. As a result, the *n*-estimators = 200, min samples split = 4, and max depth = 8 hyperparameters have been chosen for the standalone RF. However, prior to executing the constructed RF-models, the control parameters of the nature-inspired algorithms have to be chosen. Table 4 lists the control parameters that were considered for the three nature-inspired algorithms used, i.e., PSO, ACO and WOA. Furthermore, the fitness

Table 4
The utilized control parameters of the three nature inspired algorithms.

Algorithm	Parameter	Value
PSO	Number of particles	50
	c_1, c_2	2.05
	χ	0.729
	Maximum number of iterations	100
ACO	Population size	50
	Archive Size	50
	Selection probability	0.5
	Maximum number of iterations	100
WOA	Number of whales	50
	a	2 to 0 (decreasing)
	r	[0, 1]
	Maximum number of iterations	100

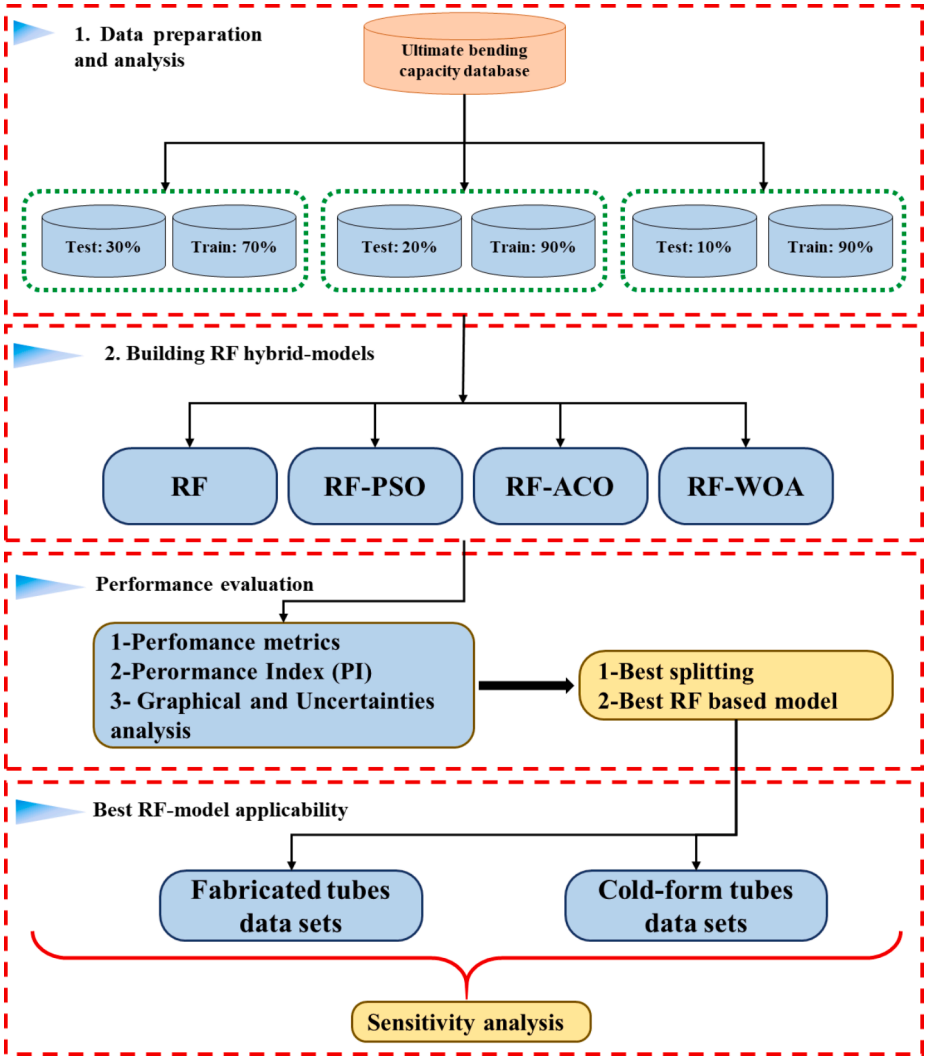

Fig. 4. Proposed framework for modeling the ultimate bending capacity in steel circular tubes.

function used throughout the optimization process is expressed mathematically as follows:

$$\min f = \sqrt{\frac{1}{n}\sum_{i=1}^{n}(E_i - P_i)^2} \quad (17)$$

where n is the number of samples utilized in the training sets, and E_i and P_i denote the experimental (ground truth values) and predicted values obtained throughout the training process.

3.3.1.3. Analysis of the results. The results of the RF-models will be compared to the actual experimental values using various statistical assessment criteria, which are described in the following section. In addition, several graphical analyses are carried out to clearly demonstrate the RF-models' effectiveness and performance. At the outset, the primary purpose is to explore the impact of data set splitting on the performance of RF-models. The optimal data set splitting and the RF-model with the highest performance may then be derived based on the findings of this stage.

3.3.1.4. Comparative analysis. The ultimate pure bending database is separated into two datasets: ultimate bending for cold-formed tubes (49 data sets) and fabricated tubes (55 data sets), which are then split into training and testing data sets based on the selected splitting scheme. The top performing RF-model is then utilized to model each of the datasets, and the results are compared to the previously established standards and the artificial neural network (ANN). Finally, the relevancy factor is used to analyze the impact of each variable on the prediction outcomes.

3.3.2. Performance analysis criteria

Different statistical assessment criteria and graphical error analysis were used to compare the performances of the proposed RF, RF-PSO, RF-ACO and RF-WOA models. Table 5 summarizes the mathematical descriptions of the statistical assessment criteria used in this study. It is worth noting that, when compared to the other models' performance, the model with the highest efficiency and accuracy should have values of RMSE, MAE closest to zero, CI and R values closest to the unit, and the lowest values of U95 and PI.

4. Results and discussion

This study primarily analyzed and compared the prediction performance of three hybrid RF-models, namely RF-PSO, RF-ACO, and RF-WOA, based on experimental databases during the training and testing phases in order to investigate an intelligent prediction model that is more suitable for practical engineering problems such as modeling the ultimate bending capacity of circular tubes. Furthermore, the comparison procedure includes the performance of a regular (unoptimized) RF model to investigate the effect of the suggested *meta*-heuristic algorithms, PSO, ACO, and WOA on the RF prediction performance. The outcomes and discussions from the comparison procedure are provided in the sections that follow.

4.1. Analysis of prediction performance

During the training and testing phases of the RF-models, each hybrid model can acquire three alternative results based on the selected splitting scheme as 90–10 %, 80–20 %, and 70–30 %, between training and testing data, respectively. The modeling strategy mentioned in Section 3.3 and depicted in Fig. 4 is employed, while results are used in this study to compare the hybrid RF-model's performance. Table 6 shows the performance of the RF-PSO, RF-ACO, and RF-WOA models, as well as the regular RF model, for the prediction of the ultimate pure bending capacity of circular steel tubes utilizing the three schemes for data splitting throughout the training and testing phases. As mentioned in Section 3.2, evaluation of the results comprise seven metrics: RMSE, MAE, U95, R^2, CI, NSE, and d.

According to the results shown in Table 6, it is clear that by using any of the three examined *meta*-heuristic algorithms (PSO, ACO or WOA) for RF optimizing, the values of all statistical indicators were better than the ones of unoptimzed RF, for any of the three splitting schemes. Thus, it is demonstrated that RF-PSO, RF-ACO, and RF-WOA can achieve higher prediction accuracy while also being more feasible and reliable models in processing datasets and applying them to engineering applications, in comparison to the unoptimized RF basic prediction.

Based on the results presented in Table 6, a trend in the performance of RF-models was seen utilizing all the three splitting schemes. The RF-WOA model clearly outperforms the RF-PSO and RF-ACO models during both stages (Training and testing). Specifically, when the second

Table 5
Statistical assessment criteria for the performance analysis.

Statistical index	Abbreviation	Mathematical formulation
Root mean squared error	*RMSE*	$\sqrt{\frac{1}{n}\sum_{i=1}^{n}(E_i - P_i)^2}$
Mean absolute error	*MAE*	$\frac{1}{n}\sum_{i=1}^{n}\lvert E_i - P_i\rvert$
Confidence Index	*CI*	$CI = WI \times NSE$ where: $NSE = 1 - \frac{\sum_{i=1}^{n}(E_i - P_i)^2}{\sum_{i=1}^{n}(E_i - \overline{E})^2}$ $-\infty \le NSE \le 1$ $d = 1 - \frac{\sum_{i=1}^{n}(E_i - P_i)^2}{\sum_{i=1}^{n}(\lvert P_i - \overline{E}\rvert + \lvert E_i - \overline{E}\rvert)^2}$ $0 \le d \le 1$
Determination Coefficient	R^2	$R^2 = \frac{\sum_{i=1}^{n}(P_i - \overline{P})(E_i - \overline{E})}{\sqrt{\sum_{i=1}^{n}(P_i - \overline{P})^2 \cdot \sum_{i=1}^{n}(E_i - \overline{E})^2}}$
Uncertainty at 95 %	U_{95}	$1.96\sqrt{SD^2 + RMSE^2}$
Performance index	*PI*	$\frac{1}{7}\left(\frac{RMSE_{model}}{RMSE_{max}} + \frac{MAE_{model}}{MAE_{max}} + \frac{U95_{model}}{U95_{max}} + \frac{R^2{}_{min}}{R^2{}_{model}} + \frac{NSE_{min}}{NSE_{model}} + \frac{WI_{min}}{WI_{model}} + \frac{CI_{min}}{CI_{model}}\right)$

E_i: Experimental value of the i-th ultimate bending moment (kN•m).
P_i: Predicted value of the i-th ultimate bending moment (kN•m).
$\overline{E}$: Average value of the ultimate bending moment (kN•m).
n: Sample's number (i.e. training and testing phases).

Table 6
Values of comparative statistical error metrics derived from predictive RF-models.

		Training phase				Testing phase			
Splitting (%)	Comparative criteria	RF	RF-PSO	RF-WOA	RF-ACO	RF	RF-PSO	RF-WOA	RF-ACO
90 %–10 %	RMSE	126.8271	88.5974	43.5959	64.0140	274.7804	247.1491	199.3295	222.3227
	MAE	60.4788	43.0566	22.5210	29.1317	113.4726	104.2755	86.9375	95.0216
	U_{95}	248.5859	174.4521	86.8547	127.0899	557.6277	502.2509	407.9945	453.3817
	CI	0.6589	0.6908	0.7357	0.7199	0.5893	0.6198	0.6661	0.6445
	R^2	0.9311	0.9727	0.9915	0.9827	0.8221	0.8554	0.9047	0.8821
	NSE	0.9233	0.9626	0.9909	0.9805	0.8129	0.8486	0.9016	0.8775
	d	0.7137	0.7177	0.7424	0.7342	0.7249	0.7303	0.7388	0.7345
80 %–20 %	RMSE	132.7186	96.3956	44.8697	85.2577	217.5238	148.0406	93.0851	133.0691
	MAE	53.4236	38.3015	18.8903	32.7959	129.9829	80.7966	47.2865	58.6252
	U_{95}	260.0740	185.6916	89.4399	166.5307	432.8958	298.2446	185.1917	263.2051
	CI	0.6779	0.6801	0.7290	0.6836	0.6547	0.6871	0.7166	0.6884
	R^2	0.9121	0.9638	0.9913	0.9784	0.8824	0.9392	0.9784	0.9563
	NSE	0.9071	0.9510	0.9894	0.9616	0.8677	0.9387	0.9758	0.9505
	d	0.7474	0.7151	0.7369	0.7109	0.7546	0.7320	0.7344	0.7243
70 %–30 %	RMSE	198.4435	177.8823	141.5637	150.0108	115.7638	102.4263	94.3032	98.2099
	MAE	97.8762	87.7603	60.4666	60.2219	51.3355	53.2185	40.6738	44.3155
	U_{95}	388.4130	345.4341	274.9827	292.9715	231.5674	203.6119	187.5606	196.5091
	CI	0.5964	0.6137	0.6501	0.6455	0.5911	0.5987	0.6709	0.6353
	R^2	0.8734	0.9102	0.9511	0.9378	0.8313	0.8836	0.9280	0.9017
	NSE	0.8604	0.8878	0.9289	0.9202	0.8312	0.8678	0.9254	0.8963
	d	0.6932	0.6913	0.6998	0.7015	0.7111	0.6898	0.7249	0.7088

scenario (80–20 %) is used for the model construction, the scores of all indicators provided by RF-WOA are the highest in the training and test phases. Notably, during the training phase, RF-WOA produced an R^2 = 0.99, RMSE = 44.87 kN•m and U_{95} = 89.44, while during the testing phase the corresponding results were R^2 = 0.98; RMSE = 93.09 kN•m and U_{95} = 185.19, demonstrating the strong ability to properly predict the final pure bending capacity of circular steel tubes. The results of the RF-ACO model were slightly better than those of the RF-PSO models, with a difference of 11.55 % and 10.11 % in terms of RMSE, 10.32 % and 11.75 % in terms of U_{95}, and 1.51 % and 1.82 % in terms of R^2 in the training and testing phases, respectively.

Obviously, the situation is different in the case of the three splitting schemes, where the obtained results of the RF-models vary from case to case and from training to testing phases. Due to the usage of the majority of the data in the model's development during the training phase, the 90–10 % scenario was able to create the RF-models with the highest performance throughout the training phase (90 %, i.e., 94 samples). However, among the other splitting schemes, the results obtained during the testing phase are the lowest. On the other hand, employing 70 % of the data for training the RF-models results in the lowest performance, as shown in Table 6 based on the error metrics. It can be noted that training the RF-models with only 80 % of the data yields results that are roughly comparable to the 90 % situation. The best testing results vary depending on the RF-model employed and the 20 % and 30 % data set scenarios for evaluating and developing the hybrid RF-models. As a result, employing diverse measuring indicators (e.g., seven metrics) cannot offer a reliable judgment on the best splitting to take for the hybrid RF-models development. As a consequence, adopting a global statistical indicator is more appropriate for providing overall findings.

Fig. 5 shows the performance index (PI) results for the hybrid RF-models during the training and testing phases. The better the model, the lower the value of PI in general. When these data are compared, it is clear that the 90 % and 80 % cases offer the best outcomes during the training phase, while the 70 % and 80 % cases provide the best results during the testing phase. It was also discovered that employing 80–20 % with the RF-WOA produced the best overall performance for predicting the ultimate pure pending of circular steel tubes, with PI values of 0.6886 and 0.7698 for the training and testing phases, respectively.

4.2. Graphical and uncertainty analysis

The cross-plot diagrams of the measured versus predicted values of the ultimate pure bending capacity for circular steel tubes throughout the training and testing stages are displayed in Fig. 6, to further analyze the performance differences between the RF model and the three hybrid RF-models. In these figures, the R^2 values for each RF-model are provided, as well as the linear connection between the measured and predicted values, indicated by the dashed black line (e.g., $Y = aX + b$, where a = 1 and b = 0 for perfect agreement). According to the graphical findings in Fig. 6, applying *meta*-heuristic algorithms greatly improves the performance of the unoptimized RF-model, with an improvement rate of 5.5 %, 6.6 %, and 8.8 % using PSO, ACO, and WOA, respectively.

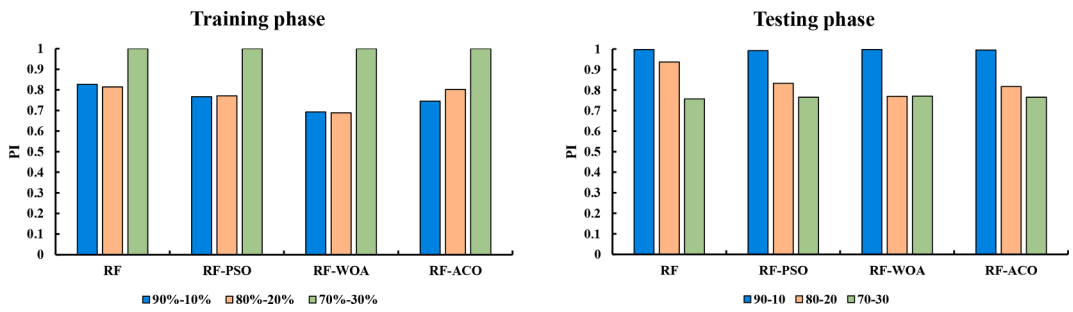

Fig. 5. PI predictive values versus data set splitting using the RF-models.

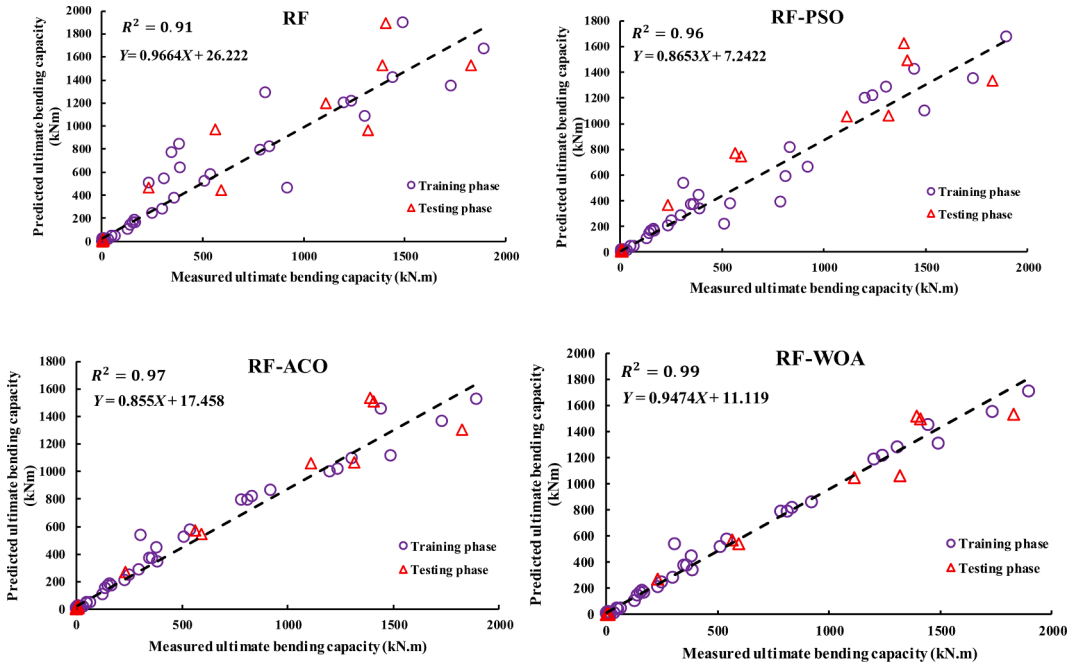

Fig. 6. Measured versus predicted ultimate pure bending values using the hybrid RF-models.

Overall, all of the RF, RF-PSO, RF-ACO, and RF-ACO predictive models performed well; however, the RF-WOA model displayed superior generalization capabilities.

The predicted to measured (*P/E*) ratio is used to highlight the uncertainty resulted by the training and testing phases throughout the modeling process. In Fig. 7, the predicted to measured (*P/E*) ratios using the results of the RF-models are presented, with each subfigure reporting the mean and standard deviation for each phase. The closer the mean values are to the unit, the lower the supplied uncertainties, and the closer the standard deviation (SD) values are to 0, the lower the data dispersion. It can be observed that the RF-WOA model has the lowest mean and SD values, with an overall mean of 1.447 and SD of 1.269, followed by the RF-ACO (MEAN = 1.522 and SD = 1.407) and RF-PSO (MEAN = 1.461 and SD = 1.694) models. The unoptimized RF-model produces the poorest results, with a mean of 1.618 and a standard deviation of 1.728. As a result, it is possible to infer that the WOA *meta*-heuristic algorithm is capable of providing the optimal search process for the RF control parameters in order to generalize its performance and improve its prediction capabilities.

4.3. Comparative analysis of the RF-WOA model

Based on the results shown above, the RF-WOA model demonstrated the highest accuracy and efficiency for estimating the ultimate pure bending capacity using the database specified in Section 2. Therefore, the RF-WOA model is utilized to predict the ultimate pure bending capacity of the cold-formed and fabricated tubes independently. As a result, the database is divided into two sections: cold formed tubes

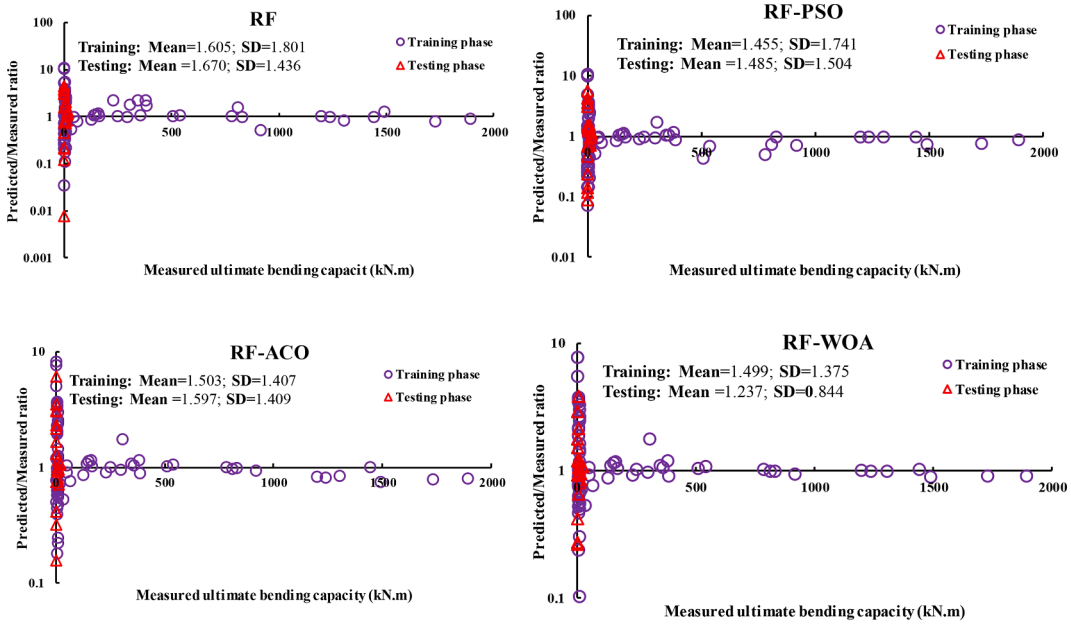

Fig. 7. Predicted to measured *(P/E)* ratios using the hybrid RF-models.

datasets and fabricated tubes datasets, as explained in details in Section 2. The RF-WOA model is then utilized to estimate each data set. It is worth noting that for each data set, an 80–20 % random division is employed. Fig. 8 depicts the cross-plot diagrams for the cold form and manufactured-fabricated- tubes in the training and testing stages, similar to Fig. 6, and the R^2 values are presented for each phase. Clearly, the RF-WOA achieves strong prediction results for both databases, with an R^2 value of 0.98 for cold formed tubes and 0.97 for manufactured tubes. It is worth noting that the performance of the RF-WOA model in the training phase was similar to that in the testing phase, showing the suggested hybrid RF-strong model's skill in sketching the ultimate bending behavior based on the available databases.

Examining the performance accuracy of the suggested hybrid RF-model (i.e. RF-WOA) against the existing standards and AI-models in the literatures is just as crucial as demonstrating prediction improvements. To evaluate the performance of the RF-WOA against the ANN, AISC, AS4100, AS/NZS 4600, and Eurocode 3 models, the normalized mean absolute error, *NMAE* ($NMAE = \frac{MAE}{\overline{E}}$) and normalized root mean squared error, *NRMSE* ($NRMSE = \frac{RMSE}{\overline{E}}$) are used. The model with the lowest *NMAE* and *NRMSE* scores is the one with the highest performance. Fig. 9 depicts the *NMAE* and *NRMSE* results for the cold-form and fabricated tubes. It should be noted that the results of the other models are derived from [32]. The suggested RF-WOA model clearly has the lowest *NMAE* and *NRMSE* values for both types of circular steel tubes, showing the strongest performance among the other models. For the cold form and fabricated tube data sets, the RF-WOA provides *NMAE* = *0.05* and *0.15*, and *NMRSE* = *0.06* and *0.25*, respectively.

Another difference is that the RF-WOA performance on cold-form datasets is slightly better than the one on fabricated datasets, which may be due to the fact that the cold-form database (i.e. 55 data points) is slightly larger than the fabricated database (i.e. 49 data points). Another finding is that the datasets in the cold-form tubes database are more closely scaled in term of the input and output variables than those in the fabricated tubes database.

4.4. Sensitivity analysis

As the database used in this study comprises actual experimental data sets, each of the four input parameters has a different impact on determining the ultimate pure bending capacity of circular steel tubes. Comparing these input variables, some had a significant influence on the prediction findings. It is crucial to explore the link between various features and final ultimate bending strength. As a result, in order to offer a preliminary explanation of the prediction process, it is critical to explore the link between these features and ultimate bending capacity (i.e. target output), as well as to establish the order of significance of these characteristics. In this study, the hybrid RF-WOA model's important order chart based on the relevancy factor (*r*), expressed in Eq. (18), is chosen to depict the importance order of the input variables for the prediction of the ultimate bending capacity of circular steel tubes [61].

$$r(I_j, O) = \frac{\sum_{i=1}^{n}(I_{j,i} - \overline{I}_j)(O_i - \overline{O})}{\sqrt{\sum_{i=1}^{n}(I_{j,i} - \overline{I}_j)^2 \sum_{i=1}^{n}(O_i - \overline{O})^2}} \tag{18}$$

where I_j is the *j*-th model inputs. $\overline{I}_j$ and $I_{j,i}$ represent I_j average value and *j-th* input value, respectively. O, $\overline{O}$ represent the estimated value and its average, respectively. A high *r* value given by a particular input parameter implies a greater influence on the ultimate bending capacity, while the *r* sign reflects the proportionality between the input variables and ultimate bending capacity. Fig. 10 illustrates the *r* values reflecting the relevance of the input variable derived from the RF-WOA hybrid prediction utilizing the overall, cold-from tubes, and fabricated tubes databases. It can be shown that various data portions result in varied *r* values, however the wall-thickness and diameters are the main influential parameters in all situations. Because of the stability of the values of the variables, as mentioned in Section 2, the Young's modulus has low influence on the eventual outcome. The rationale for the large *r* values of *E* for the constructed tube data sets is due to the input and output variable scale. This result is consistent with previous experimental studies in this regard [62–64], but it is subject to variation if a larger database with more input variables and more simulation and experimental results is used, because the used database is limited to 104 samples.

5. Conclusions

Due to the intricacy of the behavior of circular steel tubes exposed to pure bending, accurately measuring the ultimate bending capacity has always been critical for maintaining structural safety. In this work, three nature-inspired algorithms, namely PSO, ACO, and WOA were employed to optimize the parameters of the Random Forest model in order to identify more plausible parameter combinations. To that goal, a large database of experimental tests collected from both manufactured (i.e. fabricated) and cold-form steel tubes was used to correctly determine the ultimate pure bending capacity. To compare the efficiency of nature-inspired algorithms, the same population size (i.e. 50) and number of iterations (i.e. 50) were assigned to each method. Then, during the training and testing phases of the hybrid RF-models, three distinct splitting schemes were investigated: 90–10 %, 80–20 %, and 70–30 % to demonstrate the random splitting impact on model performance and to choose the ideal splitting scheme. In addition, the performance of the hybrid RF-models described in this study is determined using eight statistical measures and various graphical illustrations. Based on the findings of the study, the following are the key conclusions:

- According to the results, the hybrid RF-based models outperformed the single RF model during both phases of training and testing.
- Based on the usage of multiple performance indicators, notably the Performance Index (PI), the 80–20 % scheme revealed the ideal splitting size for training and testing the hybrid RF-Models, with PI = 0.6886 for the training and PI = 0.7698 for the testing sets, respectively.

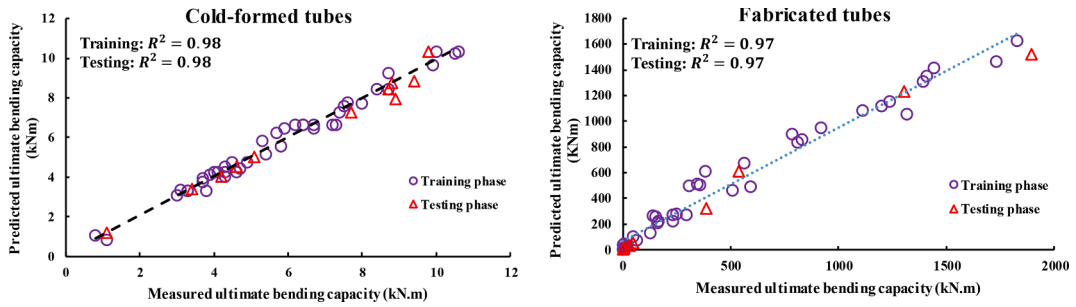

Fig. 8. Measured versus predicted ultimate pure bending capacity values for cold-formed and fabricated tubes using RF-WOA model.

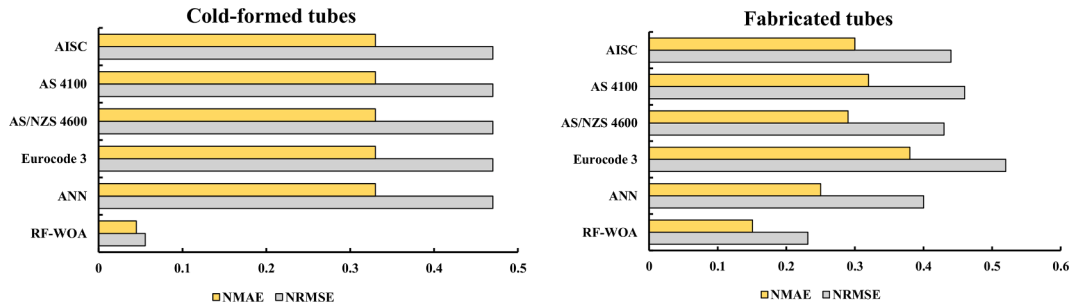

Fig. 9. Comparative NMAE and NRMSE values using RF-WOA, existing codes and models.

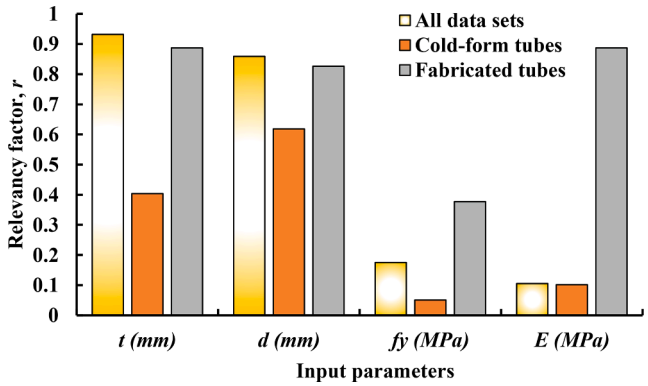

Fig. 10. Relevancy factor results.

- When the hybrid RF-models were compared, the RF-WOA model clearly outperformed the others in predicting the ultimate pure bending capacity. The RF-WOA model, in particular, produced the highest R^2 values ($R^2_{Train} = 0.9913$ and $R^2_{Train} = 0.9784$) and the lowest RMSE values ($RMSE_{train} = 44.87kN.m$ and $RMSE_{train} = 93.09kN.m$).
- According to the NMAE and NRMSE findings, the RF-WO model is assessed to be superior to pre-existing models employed for modeling the ultimate bending capacity, for both the cold-form and manufactured tubes (Cold form tubes: NMAE = 0.05, NRMSE = 0.06; Fabricated tubes: NMAE = 0.15, NRMSE = 0.25).
- In addition, the relevance order of the input variables is established based on the relevancy factor (r), which may directly show the links between the input variables and the ultimate bending capacity. According to the findings, the wall thickness and diameter have the largest influence on the final bending capacity of circular steel tubes.

The results obtained with the proposed hybrid-framework are very satisfactory. The current study, however, covers a relatively small database, which should be expanded using more experimental tests and numerical simulation, for further enhancement. Furthermore, future research should look into the relationship between the ultimate bending capacity and ovalization data. In terms of modeling, the proposed RF-WOA model can be an effective tool for modeling the ultimate bending capacity, which can then be compared to deep learning techniques in future studies.

Declaration of Competing Interest

The authors declare that they have no known competing financial interests or personal relationships that could have appeared to influence the work reported in this paper.

References

[1] Han L-H, Li W, Bjorhovde R. Developments and advanced applications of concrete-filled steel tubular (CFST) structures: Members. J Constr Steel Res 2014;100:211–28. https://doi.org/10.1016/j.jcsr.2014.04.016.
[2] Elchalakani M, Zhao XL, Grzebieta RH. Plastic mechanism analysis of circular tubes under pure bending. Int J Mech Sci 2002;44(6):1117–43. https://doi.org/10.1016/S0020-7403(02)00017-6.
[3] Hajjar JF. Concrete-filled steel tube columns under earthquake loads. Prog Struct Mat Eng 2000;2(1):72–81. https://doi.org/10.1002/(SICI)1528-2716(200001/03)2:1%3C72::AID-PSE9%3E3.0.CO;2-E.
[4] Chitawadagi MV, Narasimhan MC. Strength deformation behaviour of circular concrete filled steel tubes subjected to pure bending. J Constr Steel Res 2009;65(8):1836–45. https://doi.org/10.1016/j.jcsr.2009.04.006.
[5] Dadfar B, Hesham El Naggar M, Nastev M. Ovalization of steel energy pipelines buried in saturated sands during ground deformations. Comput Geotech 2015;69:105–13. https://doi.org/10.1016/j.compgeo.2015.05.004.
[6] CEN, *EN 1993-1: Eurocode 3, Design of steel structures, Part 1*. 1993, European Committee for Standardization (CEN).
[7] Standards Australia / Standards New Zealand, *Cold-formed steel structures. AS/NZS 4600:2005*. 2005: Sydney, Australia.
[8] Standards Australia, *Steel structures. AS 4100-1998*. 1998: Sydney, Australia.
[9] AISC. Load and Resistance Factor Design Specification for Structural Steel Buildings. Chicago, USA: American Institute of Steel Construction Inc.; 1999.
[10] Shaw PK, Kyriakides S. Inelastic analysis of thin-walled tubes under cyclic bending. Int J Solids Struct 1985;21(11):1073–100. https://doi.org/10.1016/0020-7683(85)90044-7.
[11] Kyriakides S, Shaw PK. Response and stability of elastoplastic circular pipes under combined bending and external pressure. Int J Solids Struct 1982;18(11):957–73. https://doi.org/10.1016/0020-7683(82)90086-5.
[12] Ades CS. Bending, strength of tubing in the plastic range. J Aeronaut Sci 1957;24(8):605–10. https://doi.org/10.2514/8.3916.
[13] Mamalis AG, Manolakos DE, Baldoukas AK, Viegelahn GL. Deformation characteristics of crashworthy thin-walled steel tubes subjected to bending. Proc. Inst. Mech. Eng., C 1989;203(6):411–7.
[14] Yao Y, Quach W-M, Young B. Finite element-based method for residual stresses and plastic strains in cold-formed steel hollow sections. Eng Struct 2019;188:24–42. https://doi.org/10.1016/j.engstruct.2019.03.010.
[15] Sadowski AJ, Wong WJ, Li SCS, Málaga-Chuquitaype C, Pachakis D. Critical buckling strains in thick cold-formed circular-hollow sections under cyclic loading. J Struct Eng 2020;146(9). https://doi.org/10.1061/(ASCE)ST.1943-541X.0002747.
[16] Guo, C., et al., *Behaviour and design of cold-formed CHS under static pure bending through finite element analysis.* Thin-Walled Structures, 2020. 147: p. 106547 DOI: https://doi.org/10.1016/j.tws.2019.106547.
[17] Plevris V, Tsiatas G. Computational structural engineering: past achievements and future challenges. Front Built Environ 2018;4(21):1–5. https://doi.org/10.3389/fbuil.2018.00021.
[18] Ahmad, A., et al., *Compressive strength prediction of fly ash-based geopolymer concrete via advanced machine learning techniques.* Case Studies in Construction Materials, 2022. **16**: p. e00840 DOI: https://doi.org/10.1016/j.cscm.2021.e00840.
[19] Ben Seghier MEA, Gao X-Z, Jafari-Asl J, Thai D-K, Ohadi S, Trung N-T. Modeling the nonlinear behavior of ACC for SCFST columns using experimental-data and a novel evolutionary-algorithm. Structures 2021;30:692–709.
[20] Wakjira TG, Ebead U, Alam MS. Machine learning-based shear capacity prediction and reliability analysis of shear-critical RC beams strengthened with inorganic composites. Case Stud Constr Mater 2022;16:e01008.
[21] Abd AM, Abd SM. Modelling the strength of lightweight foamed concrete using support vector machine (SVM). Case Stud Constr Mater 2017;6:8–15. https://doi.org/10.1016/j.cscm.2016.11.002.
[22] Ben Seghier, M.E.A., et al., *Simulation of the ultimate conditions of fibre-reinforced polymer confined concrete using hybrid intelligence models.* Engineering Failure Analysis, 2021. **128**: p. 105605 DOI: https://doi.org/10.1016/j.engfailanal.2021.105605.
[23] Plevris V, Asteris PG. Modeling of masonry failure surface under biaxial compressive stress using neural networks. Constr Build Mater 2014;55:447–61. https://doi.org/10.1016/j.conbuildmat.2014.01.041.

[24] Asteris PG, Plevris V. Anisotropic masonry failure criterion using artificial neural networks. Neural Comput Appl 2017;28(8):2207–29. https://doi.org/10.1007/s00521-016-2181-3.

[25] Ben Seghier MEA, Keshtegar B, Taleb-Berrouane M, Abbassi R, Trung N-T. Advanced intelligence frameworks for predicting maximum pitting corrosion depth in oil and gas pipelines. Process Saf Environ Prot 2021;147:818–33.

[26] El Amine Ben Seghier, M., et al., *Prediction of maximum pitting corrosion depth in oil and gas pipelines.* Engineering Failure Analysis, 2020. **112**: p. 104505 DOI: https://doi.org/10.1016/j.engfailanal.2020.104505.

[27] Ben Seghier MEA, Corriea JAFO, Jafari-Asl J, Malekjafarian A, Plevris V, Trung N-T. On the modeling of the annual corrosion rate in main cables of suspension bridges using combined soft computing model and a novel nature-inspired algorithm. Neural Comput Appl 2021;33(23):15969–85.

[28] Mai SH, Ben Seghier MEA, Nguyen PL, Jafari-Asl J, Thai D-K. A hybrid model for predicting the axial compression capacity of square concrete-filled steel tubular columns. Eng Comput 2022;38(2):1205–22.

[29] Tran V-L, Thai D-K, Nguyen D-D. Practical artificial neural network tool for predicting the axial compression capacity of circular concrete-filled steel tube columns with ultra-high-strength concrete. Thin-Walled Struct 2020;151:106720. https://doi.org/10.1016/j.tws.2020.106720.

[30] Ben Seghier MEA, Ouaer H, Ghriga MA, Menad NA, Thai D-K. Hybrid soft computational approaches for modeling the maximum ultimate bond strength between the corroded steel reinforcement and surrounding concrete. Neural Comput Appl 2021;33(12):6905–20.

[31] Plevris, V., C.C. Mitropoulou, and N.D. Lagaros, eds. *Structural Seismic Design Optimization and Earthquake Engineering: Formulations and Applications*. 2012, IGI Global. 456.

[32] Shahin M, Elchalakani M. Neural networks for modelling ultimate pure bending of steel circular tubes. J Constr Steel Res 2008;64(6):624–33. https://doi.org/10.1016/j.jcsr.2007.12.001.

[33] Basarir H, Elchalakani M, Karrech A. The prediction of ultimate pure bending moment of concrete-filled steel tubes by adaptive neuro-fuzzy inference system (ANFIS). Neural Comput Appl 2019;31(2):1239–52. https://doi.org/10.1007/s00521-017-3108-3.

[34] Ben Seghier MEA, Höche D, Zheludkevich M. Prediction of the internal corrosion rate for oil and gas pipeline: implementation of ensemble learning techniques. J Nat Gas Sci Eng 2022;99:104425. https://doi.org/10.1016/j.jngse.2022.104425.

[35] Xu Y, Zheng B, Zhang M. Capacity prediction of cold-formed stainless steel tubular columns using machine learning methods. J Constr Steel Res 2021;182:106682. https://doi.org/10.1016/j.jcsr.2021.106682.

[36] Rodriguez-Galiano VF, Ghimire B, Rogan J, Chica-Olmo M, Rigol-Sanchez JP. An assessment of the effectiveness of a random forest classifier for land-cover classification. ISPRS J Photogramm Remote Sens 2012;67:93–104.

[37] Ao Y, Li H, Zhu L, Ali S, Yang Z. The linear random forest algorithm and its advantages in machine learning assisted logging regression modeling. J Petrol Sci Eng 2019;174:776–89.

[38] Plevris V, Papadrakakis M. A hybrid particle swarm – gradient algorithm for global structural optimization. Comput-Aided Civ Infrastruct Eng 2011;26(1):48–68. https://doi.org/10.1111/j.1467-8667.2010.00664.x.

[39] Moayyeri N, Gharehbaghi S, Plevris V. Cost-based optimum design of reinforced concrete retaining walls considering different methods of bearing capacity computation. Mathematics 2019;7(12):1–21. https://doi.org/10.3390/math7121232.

[40] Plevris V, Karlaftis MG, Lagaros ND. In: Sustainable and Resilient Critical Infrastructure Systems. Berlin, Heidelberg: Springer Berlin Heidelberg; 2010. p. 201–30.

[41] Jafari-Asl, J., et al., *Efficient method using Whale Optimization Algorithm for reliability-based design optimization of labyrinth spillway.* Applied Soft Computing, 2021. **101**: p. 107036 DOI: https://doi.org/10.1016/j.asoc.2020.107036.

[42] Sherman, D.R. Inelastic flexural buckling of cylinders. in International Conference "Steel Structures: Recent Advances and Their Application to Design". 1986. Budva, Montenegro: Elsevier.

[43] Sherman DR. Tests of circular steel tubes in bending. J Struct Div 1976;102(11):2181–95. https://doi.org/10.1061/JSDEAG.0004478.

[44] Schilling CG. Buckling strength of circular tubes. J Struct Div 1965;91(5):325–48. https://doi.org/10.1061/JSDEAG.0001335.

[45] Jirsa, J.O., et al. Ovaling Of Pipelines Under Pure Bending. in Offshore Technology Conference. 1972.

[46] Korol RM, Hudoba J. Plastic behavior of hollow structural sections. J Struct Div 1972;98(5):1007–23. https://doi.org/10.1061/JSDEAG.0003221.

[47] Elchalakani M, Zhao XL, Grzebieta RH. Plastic slenderness limits for cold-formed circular hollow sections. Aust J Struct Eng 2002;3(3):127–41. https://doi.org/10.1080/13287982.2002.11464900.

[48] Elchalakani M, Zhao X-L, Grzebieta R. Variable amplitude cyclic pure bending tests to determine fully ductile section slenderness limits for cold-formed CHS. Eng Struct 2006;28(9):1223–35. https://doi.org/10.1016/j.engstruct.2005.10.022.

[49] Breiman L. Random forests. Mach Learn 2001;45(1):5–32. https://doi.org/10.1023/A:1010933404324.

[50] Breiman L. Bagging predictors. Mach Learn 1996;24(2):123–40. https://doi.org/10.1007/BF00058655.

[51] Ho TK. The random subspace method for constructing decision forests. IEEE Trans Pattern Anal Mach Intell 1998;20(8):832–44. https://doi.org/10.1109/34.709601.

[52] Belgiu M, Drăguţ L. Random forest in remote sensing: a review of applications and future directions. ISPRS J Photogramm Remote Sens 2016;114:24–31. https://doi.org/10.1016/j.isprsjprs.2016.01.011.

[53] Kennedy J, Eberhart R. Particle swarm optimization. In: IEEE International Conference on Neural Networks. NJ, USA: Piscataway; 1995. p. 1942–8.

[54] Dorigo M, Maniezzo V, Colorni A. The ant system: optimization by a colony of cooperating agents. IEEE Trans Syst, Man, and Cybern - Part B 1996;26(1):29–41.

[55] Dorigo M, Gambardella LM. Ant colony system: a cooperative learning approach to the traveling salesman problem. IEEE Trans Evol Comput 1997;1(1):53–66. https://doi.org/10.1109/4235.585892.

[56] Kalami Heris SM, Khaloozadeh H. Ant Colony Estimator: An intelligent particle filter based on ACOR. Eng Appl Artif Intell 2014;28:78–85. https://doi.org/10.1016/j.engappai.2013.11.005.

[57] Socha K, Dorigo M. Ant colony optimization for continuous domains. Eur J Oper Res 2008;185(3):1155–73. https://doi.org/10.1016/j.ejor.2006.06.046.

[58] Dorigo, M. and T. Stützle, *Ant Colony Optimization: Overview and Recent Advances*, in *Handbook of Metaheuristics*, M. Gendreau and J.-Y. Potvin, Editors. 2010, Springer US: Boston, MA. p. 227-263. DOI: https://doi.org/10.1007/978-1-4419-1665-5_8.

[59] Mirjalili S, Lewis A. The whale optimization algorithm. Adv Eng Softw 2016;95:51–67. https://doi.org/10.1016/j.advengsoft.2016.01.008.

[60] Gharehchopogh FS, Gholizadeh H. A comprehensive survey: whale optimization algorithm and its applications. Swarm Evol Comput 2019;48:1–24. https://doi.org/10.1016/j.swevo.2019.03.004.

[61] Tonidandel S, LeBreton JM. Relative importance analysis: a useful supplement to regression analysis. J Bus Psychol 2011;26(1):1–9. https://doi.org/10.1007/s10869-010-9204-3.

[62] Shahin MA, Elchalakani MF. A new model based on evolutionary computing for predicting ultimate pure bending of steel circular tubes. J Constr Steel Res 2014;94:84–90. https://doi.org/10.1016/j.jcsr.2013.11.011.

[63] Elchalakani M, Zhao XL, Grzebieta RH. Concrete-filled circular steel tubes subjected to pure bending. J Constr Steel Res 2001;57(11):1141–68. https://doi.org/10.1016/S0143-974X(01)00035-9.

[64] Elchalakani M, Zhao X-L. Concrete-filled cold-formed circular steel tubes subjected to variable amplitude cyclic pure bending. Eng Struct 2008;30(2):287–99. https://doi.org/10.1016/j.engstruct.2007.03.025.